

Self-potential response to periodic pumping test: a numerical study

Pavel Konosavsky, Alexis Maineult, Mikhail Narbut, Konstantin Titov

▶ **To cite this version:**

Pavel Konosavsky, Alexis Maineult, Mikhail Narbut, Konstantin Titov. Self-potential response to periodic pumping test: a numerical study. Geophysical Journal International, 2017, 210 (3), pp.1901-1908. 10.1093/gji/ggx278 . hal-01579182

HAL Id: hal-01579182

https://hal.sorbonne-universite.fr/hal-01579182

Submitted on 30 Aug 2017

HAL is a multi-disciplinary open access archive for the deposit and dissemination of scientific research documents, whether they are published or not. The documents may come from teaching and research institutions in France or abroad, or from public or private research centers.

L'archive ouverte pluridisciplinaire **HAL**, est destinée au dépôt et à la diffusion de documents scientifiques de niveau recherche, publiés ou non, émanant des établissements d'enseignement et de recherche français ou étrangers, des laboratoires publics ou privés.

Self-potential response to periodic pumping test: a numerical study

Pavel Konosavsky [1], Alexis Maineult [2], Mikhail Narbut [3], and Konstantin Titov [1*]

1) St. Petersburg State University, Institute of Earth Sciences, 7-9 Universitetskaya naberezhnaya, 199034 St. Petersburg, Russia

2) Sorbonne Universités, UPMC Univ Paris 06, CNRS, EPHE, UMR 7619 Metis, 4 place Jussieu, 75005 Paris, France

3) St. Petersburg State University, Faculty of Mathematics an Mechanics, 28 Universitetskii prospect, Staryi Petergof, 198504 St. Petersburg, Russia.

* Corresponding author

E-mail: k.titov@spbu.ru

Running title: Spectral SP modelling

Intended for publication in GJI as a research paper

SUMMARY

We numerically model self-potential responses associated with periodic pumping test experiments by sequential calculation of the hydraulic response and the coupled electrical potential. We assume the pumping test experiments with a fully saturated confined aquifer. Application of different excitation functions leads to quasi-linear trends in electrical records whose direction and intensity depend on the form of the excitation function. The hydraulic response is phase shifted compared to the excitation function; the phase shift increases quasi-linearly with the distance from the pumping well. For the electrical signals, we investigated separately the cases of conducting and insulating casings of the pumping well. For the conducting casing the electrical signals are larger in magnitude than that for the insulating casing; they reproduce the drawdown signals in the pumping well at any distance from the well and exhibit any phase shift with the increased distance. For the insulating casing, the electrical signals are phase shifted and their shape depends on the distance from the pumping well. Three characteristic regimes were found for the phase shift, φ, with the increased distance and for various hydraulic diffusivity values. At small distances φ increases quasi-linearly; at intermediate distances φ attends the value of $\pi / 2$ and stay about this value (for relatively small diffusivity values); and at large distances φ attends the value of π and, stay about this value at larger distances. This behaviour of the electrical signals can be explained by two electrical sources of reverse polarity. They are (i) linear, time independent, and located at the pumping interval of the well; and (ii) volumetric, time dependent, with maximum value located in the aquifer at the distance corresponding to maximum variation of the hydraulic head magnitude with time.

We also model the variation of the amplitude and phase of the hydraulic and electrical signals with increased excitation function period, and we show the characteristic periods corresponding to transition of the periodic pumping test regime to the classical pumping test

regime, when the excitation function is considered as the step-function. This transition depends on the distance from the pumping well and the hydraulic diffusivity value of aquifer. Finally, with this modelling of saturated flow we reproduced in sufficient details the field data previously obtained by Maineult et al. (2008).

Keywords: *self-potential, harmonic pumping tests, numerical modelling*

1. INTRODUCTION

Determining the hydraulic properties of reservoirs is essential for water resource management and oil and gas prospecting. These properties (i.e., permeability, transmissivity and diffusivity) are usually estimated on the basis of pumping tests combining observations of the flow and pressure (or the hydraulic head) in the pumping well and the pressure (or the hydraulic head) in monitoring wells (e.g., Fetter 2001). These classical tests are limited regarding the characterization of local heterogeneities because of the limited number of monitoring wells. Because heterogeneities can form preferential flow passes, or constitute low permeability zones (e.g., Chandler et al. 1989), it is very important to design new pumping test methodologies, such as periodic pumping tests, for instance (e.g., Kuo 1972; Hollaender et al. 2002; Rasmussen et al. 2003; Copty & Findikakis 2004; Renner & Messar 2006; Maineult et al., 2008; Cardiff et al. 2013). In both cases (classical pumping tests and periodic pumping tests), the areas of interest are generally sparsely covered because of the high cost of drilling. Self-potential (SP) monitoring (among other geophysical methods), can complement hydraulic campaigns (e.g., Darnet et al. 2003; Rizzo et al. 2004) since they can be implemented with dense sampling network in both space and time. SP monitoring is particularly appropriate to obtain information on temporal variations of groundwater flow because it is directly sensitive to variations in the groundwater flow and chemistry (e.g., Nourbehecht 1963; Corwin & Hoover 1979; Jouniaux et al. 1999, 2009; Maineult et al. 2005, 2006; Revil & Linde 2006). Despite the potential interest to the method (e.g., Soueid Ahmed et al. 2016; Desroches & Butler 2016), to date there are scarce datasets concerning SP observation combined with periodic pumping tests (Maineult et al. 2008). Moreover, there are observations, which have not yet been fully explained, such as the long-term trend of the signal, for instance. This motivated us to study SP responses to periodic pumping test on the

basis of numerical modelling.

In this paper, we address the following questions:

a. What are typical records of the drawdown and the SP signals?

b. How the drawdowns and the SP signals depend on the flow rate shape (excitation function)?

c. What are the differences in the SP signals in the cases of conducting (metallic) casing and insulating (PVC) casing?

d. How the phase shifts of the drawdown and of the SP signals vary with distance from the pumping well, and how they depend on the hydraulic diffusivity values?

e. How amplitude and phase of the hydraulic and electric responses vary with increase of the excitation function period?

f. Can synthetic data obtained for the saturated conditions reproduce field data?

2. NUMERICAL MODELLING METHODOLOGY

Numerical modelling is based on the finite difference method. It is a three-step procedure. First, the diffusion equation,

$$\nabla \cdot (K \nabla H) = S_s \frac{\partial H}{\partial t} + q \,, \tag{1}$$

(e.g., Domenico & Schwartz 1997) is solved with appropriate (Neumann or Dirichlet) boundary conditions for the hydraulic head, H (in m). Here K is the hydraulic conductivity (in ms^{-1}), S_s is the specific storage (in m^{-1}), and q (in s^{-1}) is the source term. Then, electrical sources are calculated on the basis of previously obtained hydraulic head distribution (the right hand part of Eq. (2)).

Finally, the electrical potential is calculated by solving Eq. (2),

$$\nabla \cdot (\sigma \nabla \psi) = -L\left(\frac{1}{a}\frac{\partial H}{\partial t} + \nabla(\ln L - \ln K)\cdot \nabla H + \frac{q}{K}\right), \quad (2)$$

where σ is the electrical conductivity (in S m^{-1}), ψ is the SP (in V), L is the streaming current coupling coefficient (in Am^{-2})), and $a = K / S_s$ is the hydraulic diffusivity (in m^2s^{-1}). Equation (2) is solved subject to appropriate boundary conditions on the electrical potential (e.g., Titov et al. 2005). The procedure of solution of the differential equations is based on the finite-difference method with strictly implicit scheme (e.g., McDonald & Harbaugh 1988; Press et al. 1992, p. 839). The modelled area is broken up into rectangular cells, which are of different size. The cells size increases exponentially in the radial direction. The finite difference discretization of Eqs. (1) and (2) produces two systems of linear equations, which are solved using the Gauss-Seidel iteration procedure with over-relaxation (Press *et al.* 1992, p. 857). We model the flow and the coupled electrical potential for the saturated zone only, and we disregard any effects of the vadose zone, which can, e.g., change the frequency content of the SP signals compared to the frequency content of the hydraulic pressure (Maineult et al. 2008, Revil et al. 2008). However, we recognize that an impact of the vadose zone can be significant especially because the coupling coefficient can be affected by the water content as was shown, for instance, by Perrier & Morat (2000), Jackson (2010), Allègre et al. (2015), and Fiorentino et al. (2016). Therefore, further studies need to account the effect of the water-content of the vadose zone.

Titov et al. (2005, 2015) previously applied this technique to model SP produced by classical pumping test. The only difference in the actual modelling methodology is a very non-uniform time discretization. Because the flow rate signal presents a series of positive and negative impulses with no-pumping/injection ("no-flow") periods between the impulses, the discretization is strongly increased at the moments of sharp variation of the flow rate, and is decreased in the periods between the flow rate variations.

We considered the model with axi-symmetric geometry centered on the pumping well.

Therefore, only one side of the cross-section (Fig. 1) is discretized. For the hydraulic and electrical modelling we kept the no-flow conditions on the ground surface (top), bottom and right boundaries of the model. The bottom boundary and the right boundary of the model are located far away from the studied area in order to guarantee that the modelled system is isolated. The model bottom is located 300 m below the ground surface, where the electrical potential value is below 10^{-9} V. The right boundary is located 2808 m away from the pumping well; this distance is much larger that the radius of influence of the pumping well, and the electrical potential value at the boundary is also below 10^{-9} V. In the modelling we obtained SP relative to the potential at this boundary.

We model a confined aquifer, whose properties are defined in Figure 1, for two cases, which differs by the material of the casing of the pumping well: conducting casing (metallic) vs. insulating casing (PVC). We apply three different forms of the excitation function; we also vary the hydraulic diffusivity value of the aquifer, as well as the excitation function period. Finally, with this modelling we reproduced non-filtered field data obtained previously by Maineult et al. (2008).

3. SYNTHETIC DATA

Steel well casings generate static SP response of electrochemical nature (e.g., Castermant et al., 2008, Maineult 2016). However, this constant component has no effect on variations of the SP signals with respect to the initial state and is not subject to the modelling.

We present the data as 2 D distributions: the hydraulic head distribution (in form of the drawdowns, in meters) and the SP signals (in mV) as functions of the time starting from the beginning of the experiment are shown for two distances from the pumping well. We also present data as functions of the distance from the pumping well for different diffusivity values

and relationships between hydraulic and electrical parameters and the excitation function period.

3.1 Excitation function

First we apply an excitation function similar to that used in Maineult et al. (2008) in their field experiment: the square impulses of different polarities (5 min duration) separated by ”no flow” period of the same duration. This produces the square wave function with period of 20 min (Fig. 2 a). For the first experiment we used the diffusivity value of 2.3×10^{-2} $m^2 s^{-1}$. The shape of the drawdown near the pumping well (Fig. 2 b) is very similar to the signals obtained by Maineult et al. (2008). Also these signals are very similar to induced polarization signals recorded in the time domain: a sharp increase of the flow rate (injection) first leads to a sharp increase of the drawdown, then to a slow increase up to the end of the injection stage. During the ”no flow” period the drawdown first sharply decreases, and then slowly decays. The same behaviour can be observed for the pumping stage. With increase of the distance the shape of the drawdown changes and become similar to sinusoid (Fig. 2c) in accordance to field data obtained by Maineult et al. (2008). Moreover, a phase shift appears between the signals recorded at different distances.

At small distance from the pumping well (Fig. 2 d) the SP signals, in the case of PVC casing of the pumping well, are similar to the drawdown, but slightly smoothed. Their polarities are inversed, comparing to the drawdown because the electrokinetic coefficient $C = -L/\sigma$ is negative. With increase of the distance (Fig. 2 e), similarly to the case of the drawdown the SP signals become close to sinusoid and are phase shifted comparing to the flow at the pumping well. In contrast to the signals obtained with PVC casing of the pumping well, those obtained for the case of the metallic casing are of the same shape as the drawdown near the pumping well (regardless of the distance) and are not phase shifted.

The drawdown and the SP signals decrease with distance from the pumping well regardless on the type of the casing. In all signals (except the drawdown near the pumping well) small long-term trends are visible. These trends reflect a "history" of the excitation, namely the polarity of the first impulse (negative in the discussed experiment): the first hydraulic response is shifted toward negative values, and the first SP response is shifted toward positive values. Then with increase of the number of excitation impulses the trends tend to zero.

Then we apply a sequence of impulses of the same polarity (Fig. 3) interleaved by "no flow" period with the same duration as the impulses. This flow rate form is potentially interesting because is less time consuming than the signal containing bipolar impulses. For the same reasons a similar form of the excitation signal is also discussed for induced polarization applications (e.g., Fiandaca et al. 2016). The main features of the hydraulic and electrical records are the same, as in the previous case, however the phase shifts are slightly reduced (if exist) and the trends of the signals become appreciably larger. When the polarity of the excitation function change, all the responses also change the polarity (not shown), which is explained by the linearity of the studied system.

3.2 Phase shift vs. distance from the pumping well

We model the phase shift for the hydraulic and electrical responses with the hydraulic diffusivity value of the aquifer, a , between $2.3\text{x}10^{-3}$ m^2 s^{-1} and $2.3\text{x}10^{-2}$ m^2 s^{-1}. We use a dimensionless normalized distance from the pumping well, which is defined as $R_n = \frac{R}{\sqrt{\pi a T}}$ (T being the excitation function period (in s), and R being the distance (in m)). This normalized distance characterizes the effective pumping radius obtained with classical pumping test at the time value of T. Figure 4 shows these relationships for four diffusivities values. The phase shifts of hydraulic signal monotonously increase for all four values of the diffusivity (Fig. 4a).

Starting from the normalized distance of about 0.6 this increase becomes linear.

For the largest diffusivity value (2.3×10^{-2} $m^2 s^{-1}$) the phases shift of the electric signals, in the case of PVC casing, increase up to the value of π at the normalized distance of about 2. For the all smaller values of the diffusivity, the phase shift exhibits three different regimes. The shift values first quickly increases up to values of about $\pi / 2$ (regime I), then they stay at about $\pi / 2$ value (regime II), and then they quickly increase up to the value of about π (regime III). For the case of metallic casing of the pumping well we did not find any phase shift in the electrical signals (see Fig. 2).

3.3 Amplitude and phase vs. period

Figure 5 shows variations of the amplitude and phase of the hydraulic and electrical signals as functions of the flow rate period calculated for the aquifer diffusivity value of 2.3×10^{-2} $m^2 s^{-1}$. All the relationships were calculated for four distances from the pumping well (1.1, 4.1, 9.4 and 21.4 m). The amplitudes of drawdown are close to logarithmic function of period, especially with decrease of the distance from the pumping well, and with increase of the period (Fig. 5 a). This is in good agreement with the logarithmic approximation of the drawdown vs. time (Domenico & Schwartz 1997). We calculated the SP amplitude for the cases of metallic (Fig. 5 b) and PVC (Fig. 5 c) casings of the pumping well. For the SP signals, the magnitude increases with increased period and decreases with increased distance from the pumping well. Also the magnitude is larger for the case of metallic casing (Fig. 5 b), comparing to the case of PVC one (Fig 5 c). The phase shift of hydraulic signals monotonously decreases with increasing period (Fig. 5 d). The largest phase shift was obtained at the largest distance from the pumping well and for the smallest period value. For the distances of 1.1 m the phase shift values are very small and cannot be plotted with the used scale. With increased distances the phase shifts progressively increase. For the distances

of 4.1, 9.4 and 21 m the phase shifts approach to zero at the period values of 100, 1000 and 10000 min, respectively. At large periods the SP phase shifts (in the case of PVC casing) show very similar behaviour (Fig 5 e). Noticeably, at small periods the electrical signals phase shift was found to be close to π (R = 21.4 m) and to $\pi/2$ (R = 9.4 m). In Fig. 5 f we show all the data points shown in Figs. 5 d and 5 e. The phase shifts of the hydraulic and electrical signals are in good agreement, except two characteristic asymptotic values of the SP phase shift ($\pi/2$ and π).

4. COMPARISON OF FIELD AND MODELLED SELF-POTENTIAL SIGNALS

To validate our modelling approach and results we compare field records obtained by Maineult et al. (2008) with our synthetic data. In this model, we consider the real pumping well construction, which was cased by iron tube in the first 4.24 m. The rest of the well was cased with PVC tube. We used the sediments electrical conductivity value obtained by Maineult et al. (2008) with electrical tomography (0.05 Sm^{-1}) and we obtained the hydraulic diffusivity value of 5 10^{-2} m^2s^{-1} with trial and errors. This value is twice lower than the lower limit of the diffusivity obtained by Maineult et al. (2008). The electrokinetic coefficient was found to be –0.96 mVm^{-1}, which is roughly twice larger than the apparent electrokinetic coefficient assessed by Maineult et al. (2008). However, our aim was not to investigate the sensitivity of SP signals to hydraulic parameters but to understand if field records can be reproduced with numerical modelling considered the saturated zone only. Figure 6 shows the de-trended field electric records (Maineult et al. 2008, their Fig. 4 c, d, e,) and the modelled data, which are in reasonable agreement. We stress that the modelled data are not harmonic and they are very similar to those obtained for the case of metallic casing (see Fig. 2 f and g). The model signal attenuation is also in qualitative agreement with the field data.

5. DISCUSSION

The modelled data show small, but detectable non-linear trends whose direction is determined by the polarity of the first impulse (Fig. 2). If it is of negative polarity, the SP trend increases up to an asymptotic value corresponding to a static SP signal. Theoretically, this asymptotic value can be achieved after an infinite sequence of the impulses. This effect is well known in the time domain induced polarization method (Tarasov & Titov, 2007), and strongly increases when the excitation signals contain impulses of the same polarity (see Fig. 3).

Figure 2 shows a similarity between the SP signals and the drawdowns. Figures 7 and 8 show correlations between these signals. For the case of the metallic casing and at the shortest distance from the pumping well SP is strongly correlated with the drawdown (Fig. 7 a). The slope of the relationship, which is the apparent electrokinetic coefficient, is about three times lower than the true electrokinetic coefficient of the aquifer. This small value of the apparent coefficient comparing to that of the true coefficient is produced by the screening effect of SP by formation underlying and covering the aquifer (see Titov et al., 2005, their Fig. 9 c and d). With increased distance from the pumping well the correlation degree between the SP and drawdown strongly reduces (Fig. 7 b). We explain this fact, first, by variation in shape of the drawdown signals with increased distance from the pumping well (the drawdown vs. time relationship becomes smother). In contrast, the SP signals keep the same form (Fig. 2). Second, the drawdown signals exhibit an increased phase shift with increased distance, which is not typical for the SP signals. This phase shift (close to π, compare Fig. 2 b and c) leads to a positive value of the apparent electrokinetic coefficient (Fig. 7 b). Moreover, the apparent coefficient shows a value larger in magnitude than that of the true coefficient (26.6 mVm^{-1} vs. -8.14 mVm^{-1}). This is only possible when the casing is

made of metal. (Titov et al. (2005) modelled this effect and they have shown an increase of the SP magnitude with increased electrical conductance of the well casing (their Fig. 9 b)).

For the case of the PVC casing, and at short distance from the pumping well the relationship between SP and drawdown is non-linear and hysteretic (Fig. 8 a). We explain this behaviour by a difference in shape between the drawdown and the SP signals (Fig. 2 b and d). The strong decrease of the drawdown at the beginning of the injection phase is followed by much slower increase of the SP signal, and the fast decrease of the drawdown at the phase end leads to much slower SP decreases, which produces the non-linear relationship between the parameters. We explain this observation based on examination of the SP sources.

An inspection of Eq. (2) for the case of homogeneous aquifer reveals that two sources of electrical field are at play. One source is associated with the water pumped from and injected to the well with the intensity (in A m^{-3})

$$J_1 = \pm L \frac{q}{K}. \qquad (3)$$

It is located on the pumping well wall and is time independent. The second source appears because of the non-steady state flow, it depends on time; the source intensity is

$$J_2 = \mp \frac{L}{a} \frac{\partial H}{\partial t}. \qquad (4)$$

This second source is volumetric; its maximum magnitude approximately corresponds to the distance of $\sqrt{\pi a t}$ from the pumping well (*t* being the time counted from the beginning of the pumping or injection cycle) (e.g., Domenico & Schwartz 1997). According to the charge conservation, it is of reversal polarity comparing the source at the well (i.e., phase shifted by π).

The Green's function of the Poisson equation (2) is solution of

$$\nabla^2 G(r, r') = \delta(r'), \qquad (5)$$

where *r* and *r'* are coordinates of the observation and source points, respectively, and $\delta(r')$ is

the Dirac distribution (see, e.g., Rizzo et al. 2004).

The Greens function for a homogenous half-space is

$$G(r,r') = -\frac{1}{2\pi}\frac{1}{|r-r'|}. \qquad (6)$$

Therefore the electrical potential,

$$\psi(r) = -\frac{1}{2\pi\sigma}\int_V \frac{(J_1(r') + J_2(r')dV}{|r-r'|}, \qquad (7)$$

is the sum of two sources distributions (of inverse polarity, or phase shifted by π) weighted by the inverse distance between each source point and observation point.

If only the first source is at play, the SP signal shape would be the same as that of the flowrate record (Fig. 2 a). The second source of opposite polarity reduces the SP magnitude at the beginning of the pumping and injection stage, and produces an SP decays at the end of each stage like in records of the time domain induced polarization. The more is the diffusivity value, the more this effect is pronounced (not shown). This difference in shape between the drawdown and SP signals also leads to a hysteretic character of the respective relationship. In addition, the first impulse of the test produces a deviation compared to the subsequent impulses in the discussed relationship. With increase of the impulse number the respective graphs of the relationship become tighter, which reflects the effect of the first impulse polarity, producing the trends discussed below (see Fig. 2).

The limiting SP phase shift value of π (Fig. 4 b, Regime III) is obtained in the vicinity of the centre of the volumetric source, and the intermediate phase shift value of about $\pi/2$ (Fig. 4 b, regime II) is obtained at distances between the two above-mentioned sources.

With increase of the distance from the pumping well the correlation degree decreases (Fig. 8 b). For each impulse, the relationship presents ellipse-like geometrical figure. This effect is produced by a common impact of (i) different shape of SP and drawdown and (ii) the phase shift between these two parameters (compare Fig. 2 c and e). Application of an artificial

phase shift of 3.7 min strongly increased the correlation degree (Fig. 8 c).

In contrast to the PVC casing, for the case of metallic casing, the phase shift is zero, and, so, only the first source channelling to the surface by the conductive casing is at play. Therefore its impact to the electrical field is appreciable greater than that of the second source.

The phase shifts of hydraulic and electrical signals approach to zero with increased period of excitation (Fig. 5 d and e). When the phase values are close to zero, the pumping test come over harmonic to the standard regime when the excitation signal is the step-function. This transition starts at smaller distances from the pumping well (see Fig. 5 d and e). Despite limiting values of $\pi/2$ and π at small periods (Fig. 5 e) the phase shifts of the hydraulic and electrical responses are in strong correlation (Fig. 5 f).

6. CONCLUDING STATEMENTS

We have reproduced records of the drawdown and of the SP signals with numerical modelling of saturated flow and coupled electrical field. These signals attenuate with distance from the pumping well. The SP signals contain trends, whose direction depends on the polarity of the first impulse. For the excitation function containing signals of the same polarity, this trend strongly increases.

The SP signals are quite different depending on material of the well casing. For the case of metallic casing the signals are of greater magnitude and do not exhibit phase shift, comparing to the case of insulating casing, when the magnitude of the signals is smaller and the phase shift exists between the electrical signals and the excitation function. This phase shift is qualitatively explained by influence of two sources of different polarities and location.

We believe more experimental data need to understand the SP signals accompanying the periodic pumping test. In this paper, we did not discuss the impact of the vadose zone (as

done by Revil et al. 2008) as well as the Fourier analysis of the signals: we leave these problems for future works.

Acknowledgements

We thank the reviewers and the Associate Editor for their useful comments. We acknowledge the support of the Russian Science Foundation (grant № 17-17-01160 "Physical-chemical models of Induced Polarization and Self-Potential with application to pumping test experiments").

FIGURES

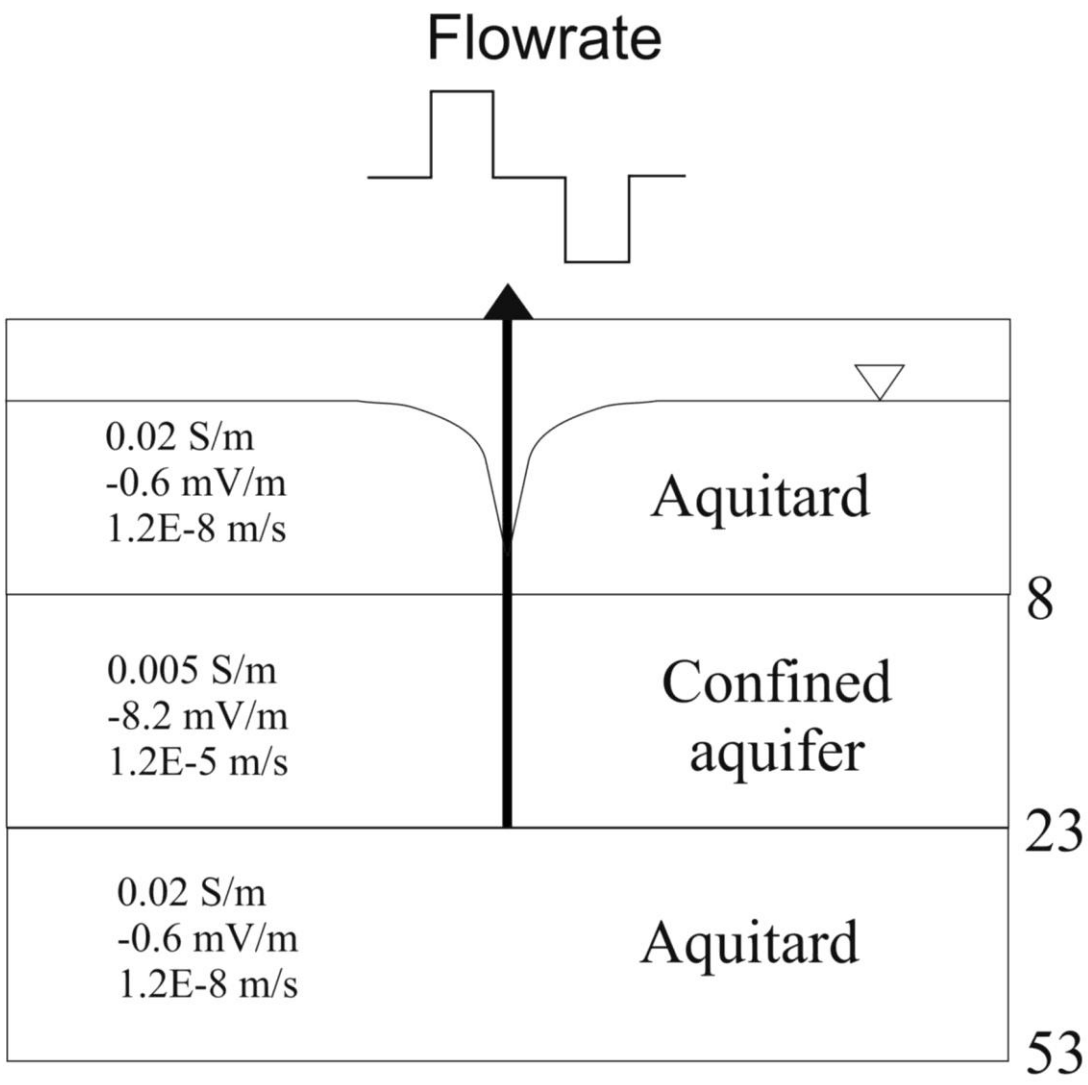


Figure 1. Sketch of the modelled pumping test experiment. Numbers show values of the electrical conductivity, the electrokinetic coefficient, and the hydraulic conductivity, respectively. We used typical values of the parameters for fresh water aquifers and for clayey aquitards. The pumping/injection well can be with conductive (metallic) and isolating (PVC) casings. For the modelling of field data (Fig. 6) we suppose first 4.25 m of the casing was made of metal and the rest was made of PVC.

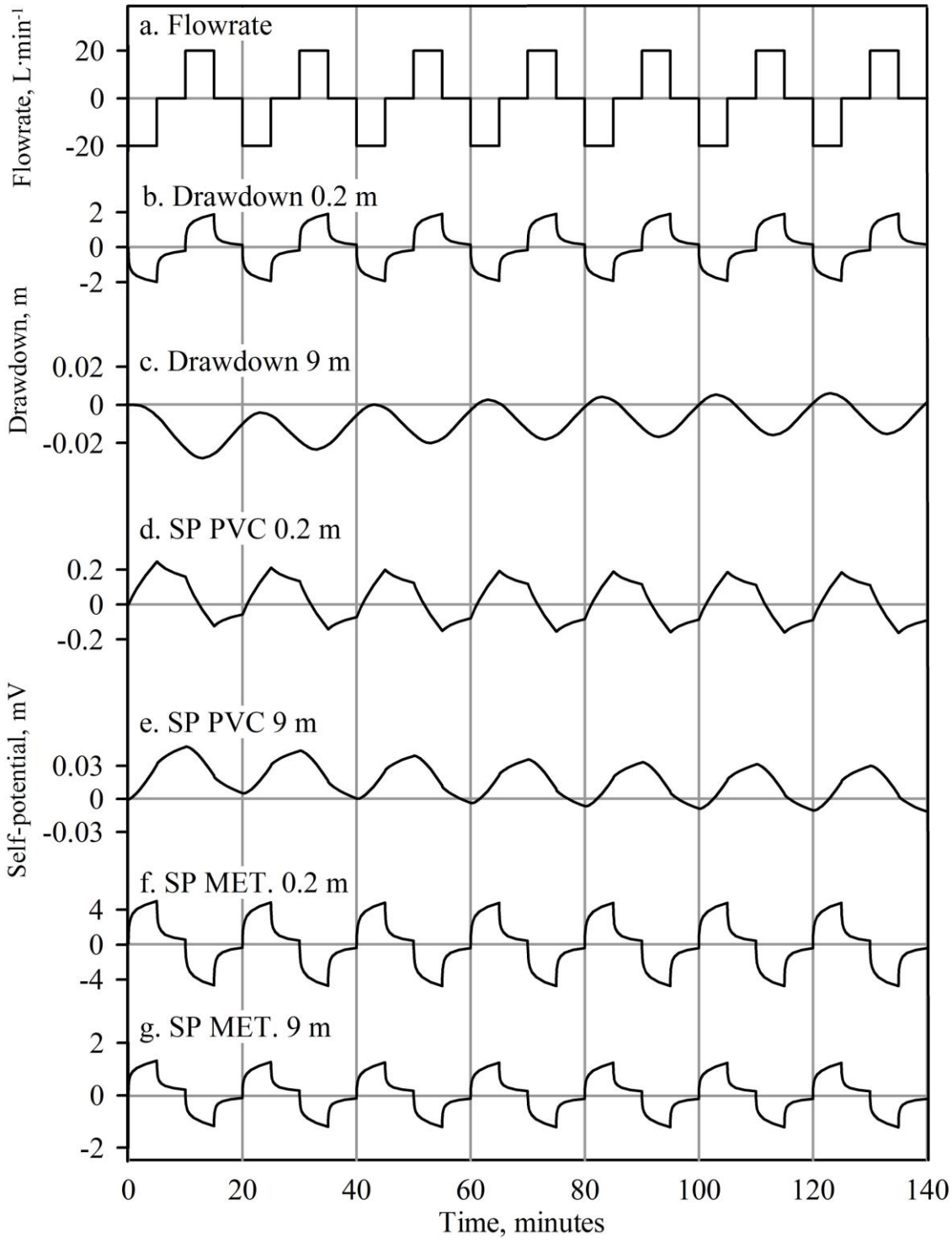


Figure 2. Typical modelled signals vs. time near the pumping well (0.2 m), and at distance 9 m. The signal period is 20 min; the hydraulic diffusivity is 2.3×10^{-2} m^2 s^{-1}. **a**: flow rate; **b**, **c**: drawdown at 0.2 m and 9 m, respectively; **d**, **e**: self-potential signals at 0.2 m and 9 m, respectively (PVC casing); **f**, **g**: self-potential signals at 0.2 m and 9.4 m, respectively (metallic casing).

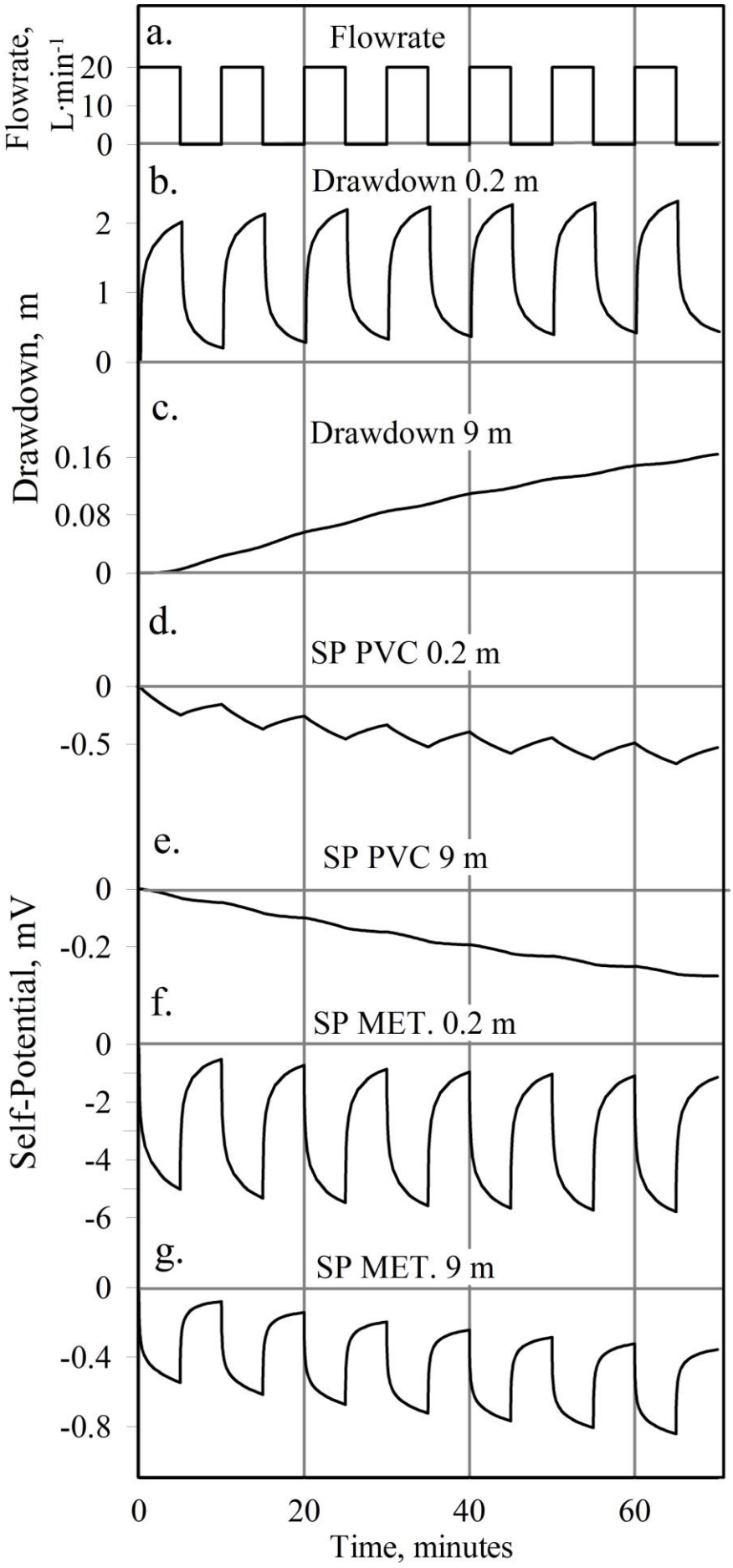

a.
Flowrate
Flowrate, L·min-1
20
10
0
b.
Drawdown 0.2 m
2
1
0
Drawdown, m
c.
Drawdown 9 m
0.16
0.08
0
d.
SP PVC 0.2 m
0
-0.5
e.
SP PVC 9 m
0
-0.2
f.
SP MET. 0.2 m
0
-2
-4
-6
g.
SP MET. 9 m
0
-0.4
-0.8
Self-Potential, mV
0
20
40
60
Time, minutes

Figure 3. Influence of the form of the excitation function on the drawdowns and SP signals. The signal period is 20 min., the hydraulic diffusivity is 2.3x10-2 m^2 s^{-1}. **a**: excitation function; **b** and **c**: the drawdown at the distances of 0.2 m and 9 m, respectively; **d** and **e**: SP signals at the distances 0.2 and 9 m, respectively (PVC casing); **f** and **g**: the same for the metallic casing.

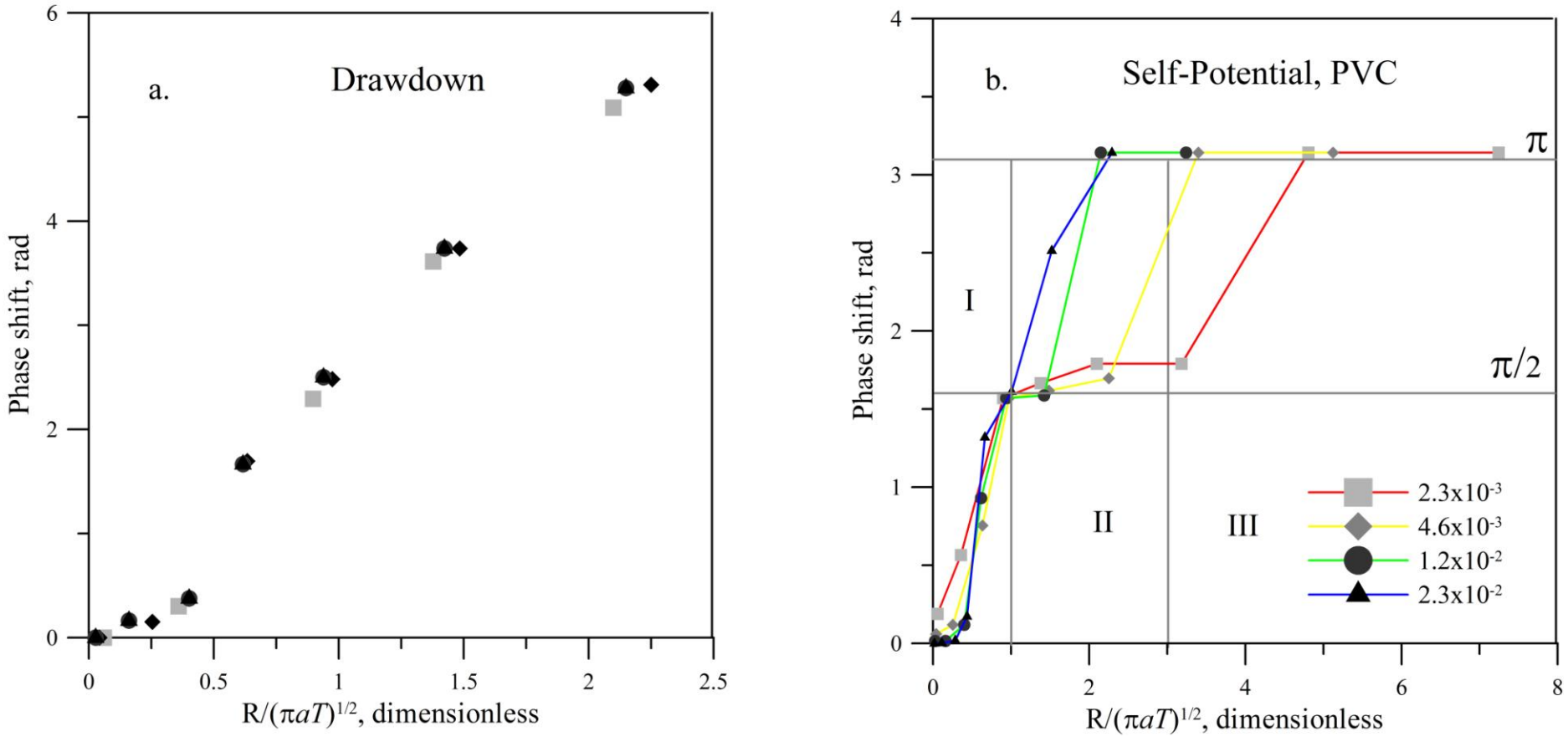
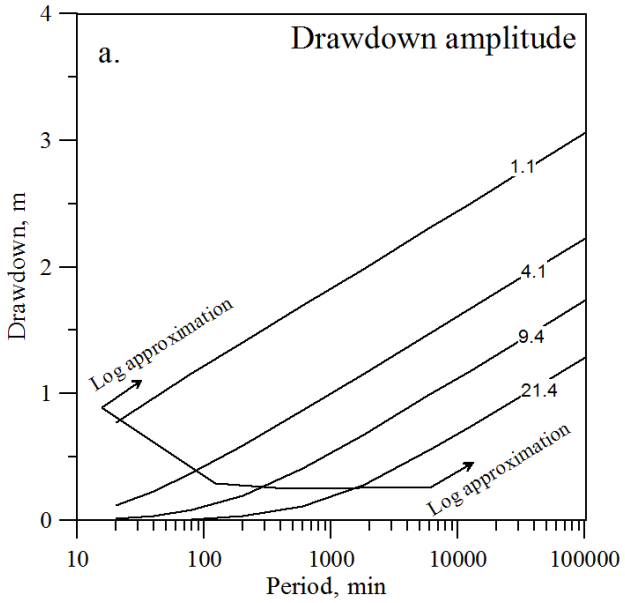
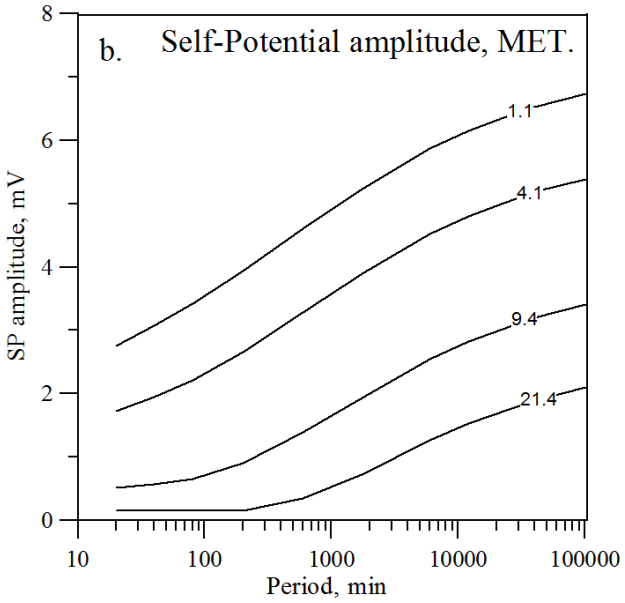
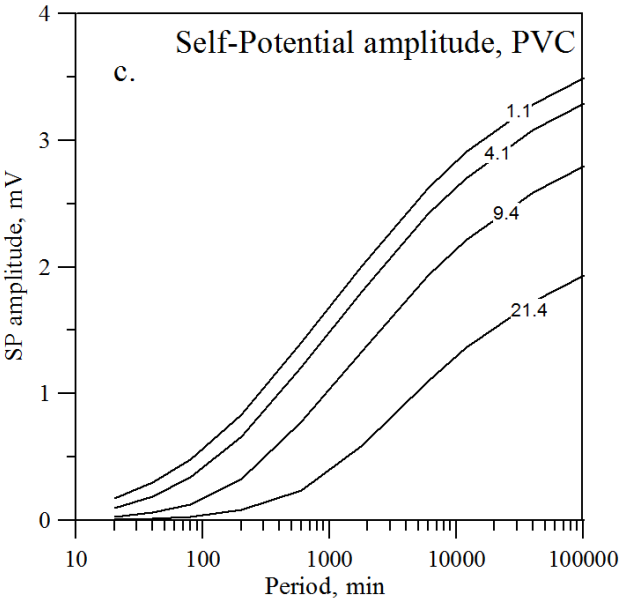


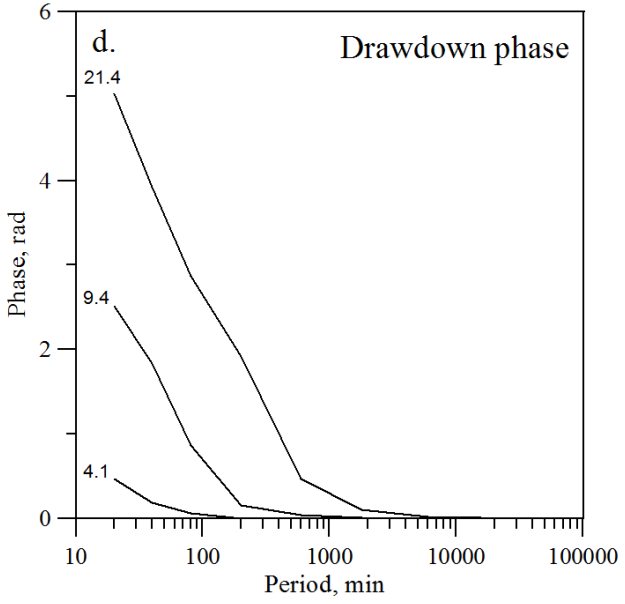
Figure 4. Phase shift between the hydraulic response and the flow rate (**a**), and between the self-potential signals and the flow rate (**b**) as functions of the normalized distance from the pumping well for different diffusivity values. The normalized distance is defined as the ratio of the distance and the characteristic radius of the pumping, which is considered as $\sqrt{\pi aT}$. For the drawdown, note a quasi-linear trend typical

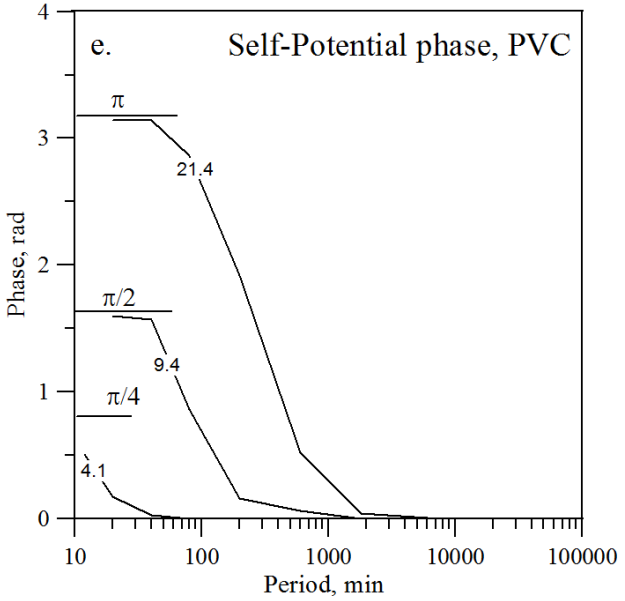
of all the diffusivity values. For SP note three characteristic regimes: a linear increase of the phase, regime I (normalized distance is from 0 to 1), a trend to the values of about $\pi/2$, regime II (normalized distance is from 1 to about 3 depending on the diffusivity value), and the trend toward the value of π, regime III (normalized distance is larger than about 3). The diffusivity values are plotted in Fig. 4 b in m^2s^{-1}.


a.
Drawdown amplitude
Drawdown, m
Period, min
1.1
4.1
9.4
21.4
Log approximation
Log approximation


b.
Self-Potential amplitude, MET.
SP amplitude, mV
Period, min
1.1
4.1
9.4
21.4


c.
Self-Potential amplitude, PVC
SP amplitude, mV
Period, min
1.1
4.1
9.4
21.4


d.
Drawdown phase
Phase, rad
Period, min
21.4
9.4
4.1


e.
Self-Potential phase, PVC
Phase, rad
Period, min
π
π/2
π/4
21.4
9.4
4.1

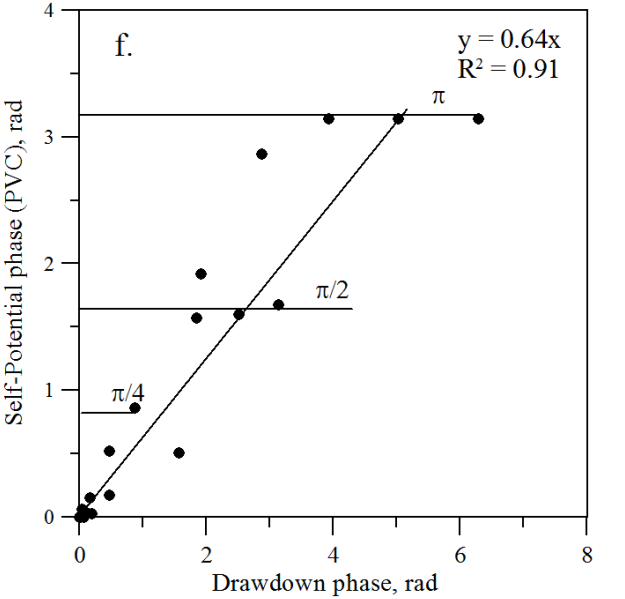

f.
y = 0.64x
R² = 0.91
Self-Potential phase (PVC), rad
Drawdown phase, rad
π
π/2
π/4

Figure 5. Amplitude of the drawdown (**a**) and the self-potential signals (**b**) and (**c**) vs. flow rate period (**b** is the case of metallic casing, and **c** is the case of PVC casing); phase shifts of the drawdown (**d**) and of the self-potential signals (**e**) vs. flow rate period (PVC casing); and relationship between the SP and hydraulic head phase shifts (**f**) for the data plotted in Figs. 5d and e.

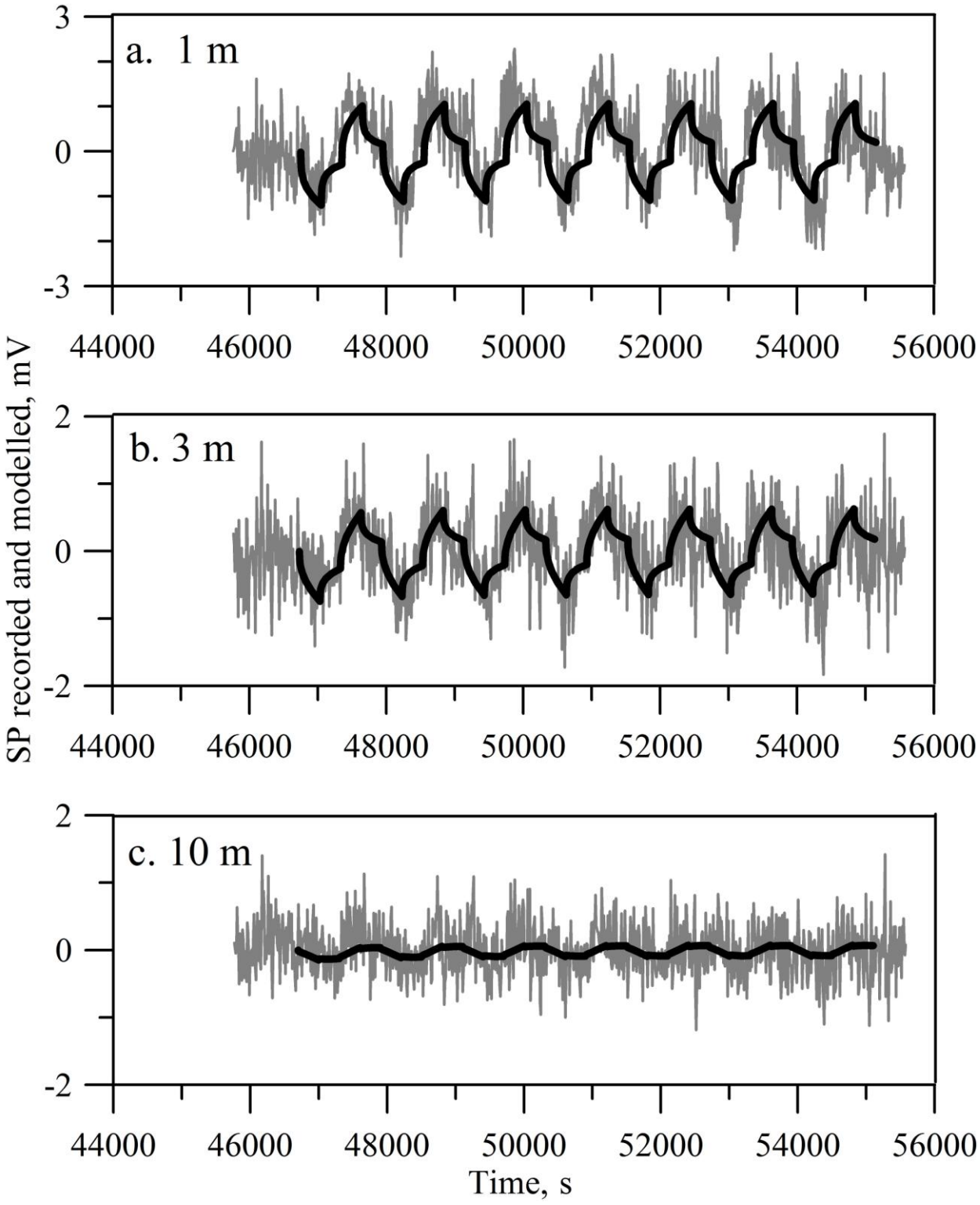


Figure 6. Comparison of recorded SP signals (Maineult et al., 2008) and modelled signals (this work) at 1, 3, and 10 m distances from the pumping well. Note in contrast to the sketch (Fig. 1) the first 4.25 m of the casing is made of metal, and the rest of the casing is made of PVC.

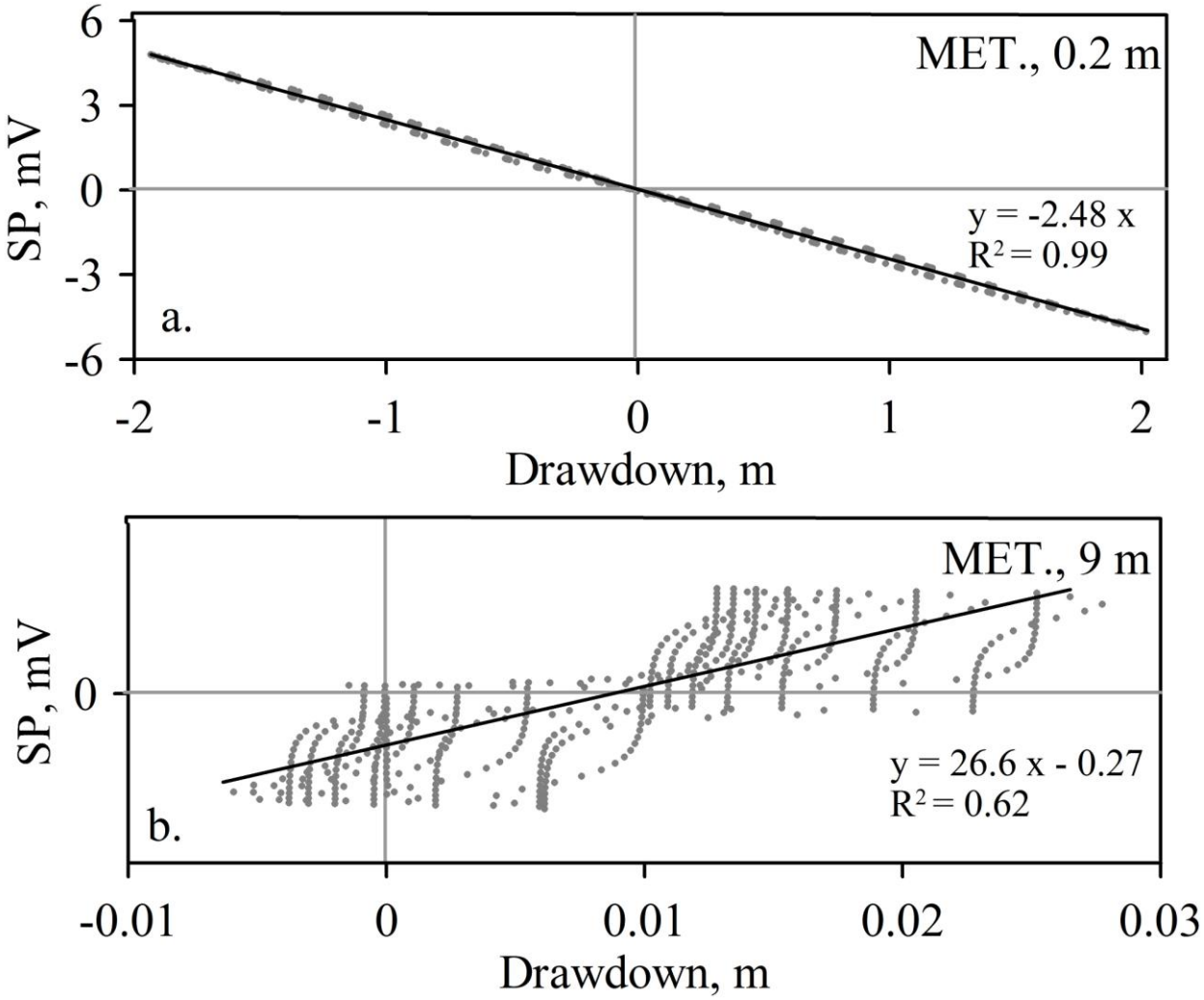


Figure 7. Self-Potential vs. drawdown at 0.2 m (**a**) and 9 m (**b**) from the pumping well; the case of metallic casing. Solid lines show the best linear fits.

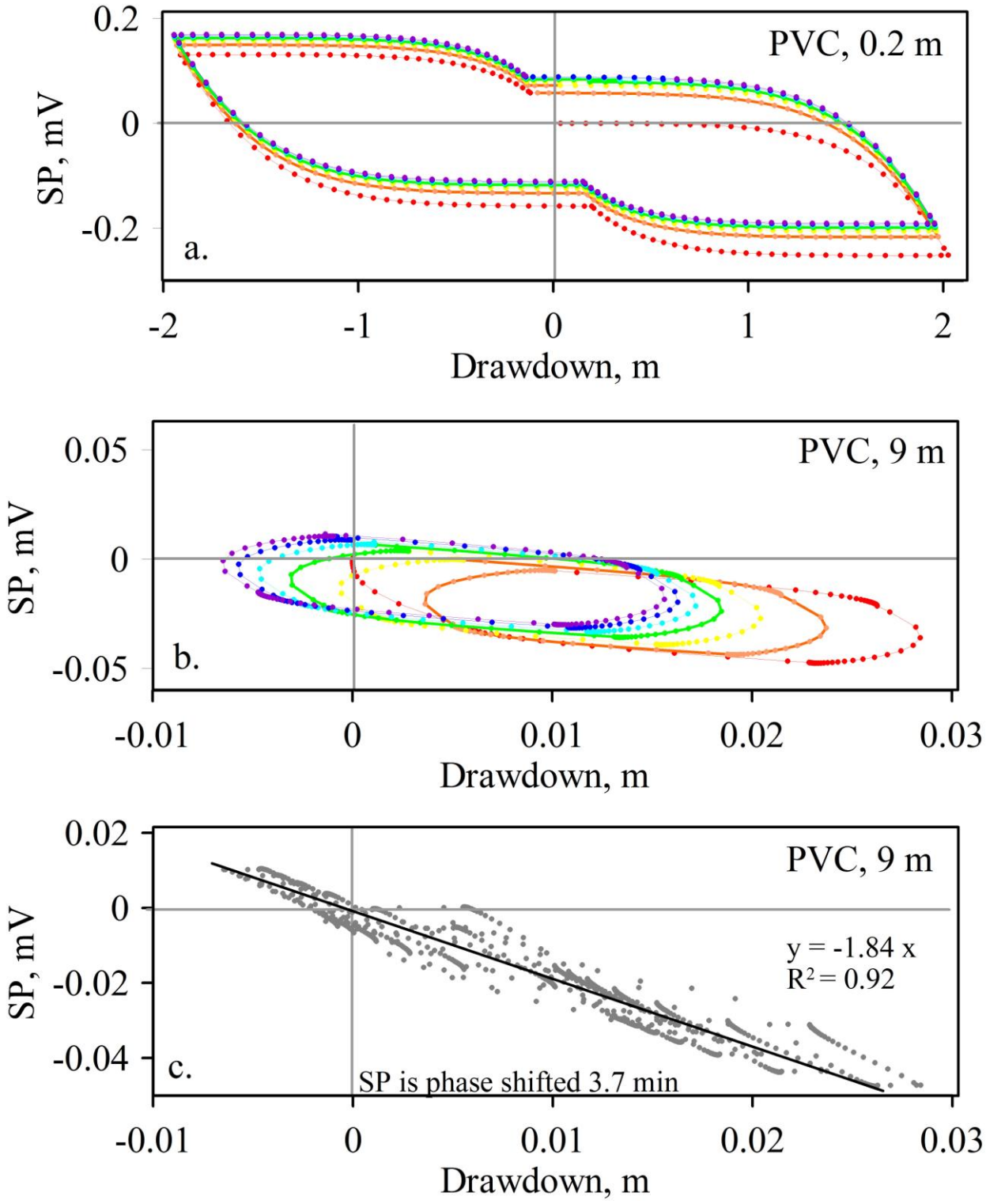


Figure 8. Self-Potential vs. drawdown at 0.2 m (**a**) and 9 m (**b**, **c**) from the pumping well; the case of PVC casing. The rainbow colours from red (the first cycle) to violet (the seventh cycle) code every cycle of the pumping /injection. Self-Potential signal is 3.7 min phase shifted relative to the drawdown (**c**). Solid line shows the best linear fit.

REFERENCES

Allègre, V., Jouniaux, L., Lehmann, F., Sailhac, P., & Toussaint, R., 2015. Influence of water pressure dynamics and fluid flow on the streaming-potential response for unsaturated conditions, *Geophysical Prospecting*, 63, 694-712.

Cardiff, M., Bakhos, T., Kitanidis, P.K. & Barrash, W., 2013. Aquifer heterogeneity characterization with oscillatory pumping: sensitivity analysis and imaging potential, *Water Resources Res*., 49, 5395–5410, doi: 10.1002/wrcr.20356.

Castermant, J., Mendonça¸ C.A., Revil, A., Trolard, F., Bourrié, G. & Linde, N., 2008. Redox potential distribution inferred from self-potential measurements associated with the corrosion of a burden metallic body. *Geophysical Prospecting*, 2008, 56, 269–282. doi:10.1111/j.1365-2478.2007.00675.x.

Chandler, M.A., Kocurek, G., Coggin, D.J. & Lake, L.W., 1989. Effects of stratigraphic heterogeneity on permeability in eolian sandstone sequence, Page sandstone, Northern Arizona, *AAPG Bull.*, **73**, 658–668.

Copty, N.K. & Findikakis, A.N., 2004. Stochastic analysis of pumping test drawdown data in heterogeneous geologic formation, *J. Hydraul. Res.*, **42**, 59–67, doi: 10.1080/00221680409500048.

Corwin, R.F. & Hoover, D.B., 1979. The self-potential method in geothermal exploration, *Geophysics*, **44**, 226–245, doi: 10.1190/1.1440964.

Darnet, M., Marquis, G., & Sailhac, P., 2003. Estimating aquifer hydraulic properties from the inversion of surface streaming potential (sp) anomalies, *Geophys. Res. Lett.*, **30**(13), 1679, doi: 10.1029/2003GL017631

Desroches, A. & Butler, K., 2016. Monitoring and modeling of pumping-induced Self-Potentials for transmissivity estimation within a heterogeneous confined aquifer, *Geophys. J. Int*., **207**(3), 1722–1738, doi: 10.1093/gji/ggw354.

Domenico, P.A. & Schwartz, F.W., 1997. *Physical and Chemical Hydrogeology*, 2nd ed., John Wiley, Hoboken, N. J.

Fetter, C.W., 2001. *Applied Hydrogeology*, 4th ed., Macmillan, New York.

Fiandaca, G., Auken E. & Christiansen, A.V., 2016. Advances in spectral inversion of time-domain induced polarization, *4th International workshop on induced polarization*, 6-8 June 2016, Aarhus, Denmark, http://hgg.au.dk/fileadmin/www.gfs.au.dk/DIV/Abstracts_from_Session_A.pdf.

Fiorentino, E., Toussaint, R., & Jouniaux, L., 2016. Two-phase lattice Boltzmann modelling of streaming potentials: influence of the gas-water interface on the electrokinetic coupling, *Geophys. J. Int.*, **208**(2), 1139–1156, doi: 10.1093/gji/ggw417.

Jackson, M. D., 2010. Multiphase electrokinetic coupling: Insights into the impact of uid and charge distribution at the pore scale from a bundle of capillary tubes model, *J. Geophys. Res*., **115**(B7), B07206, doi: 10.1029/2009JB007092.

Hollaender, F., Hammond, P. & Gringarten, A.C. 2002. Harmonic testing for continuous well and reservoir monitoring, *paper SPE 77692*, doi: 10.2118/77692-MS.

Jouniaux, L., Pozzi, J.-P., Berthier, J., & Mass_e, P., 1999. Detection of fluid flow variations at the Nankai trough by electric and magnetic measurements in boreholes or at the seafloor, *J. Geophys. Res.*, **104**(B12), 29293–29309, doi: 10.1029/1999JB900102.

Jouniaux, L., Maineult, A., Naudet, V., Pessel, M., & Sailhac, P., 2009. Review of self-potential methods in hydrogeophysics, *C.R. Geosci.*, **341**, 928–936, doi: 10.1016/j.crte.2009.08.008

Kuo, C.H., 1972. Determination of reservoir properties from sinusoidal and multirate flow tests in one or more wells, *Soc. Petrol. Eng. J.*, **12**, 499–506, doi: 10.2118/3632-PA.

McDonald, M.C. & Harbaugh, A.W., 1988. MODFLOW, A modular threedimensional finite difference ground-water flow model, *U.S. Geological Survey Open-file report*, 83–875, Chapter A1.

Maineult, A., Bernabé, Y. & Ackerer, P. 2005. Detection of advected concentration and pH

fronts from spontaneous potential measurements, *J. Geophys. Res.*, **110**, B11205, doi: 10.1029/2005JB003824.

Maineult, A., Jouniaux, L., & Bernabé, Y., 2006. Influence of the mineralogical composition on the self-potential response to advection of KCl concentration fronts through sand, *Geophys. Res. Lett.*, **33**(24), L24311, doi: 10.1029/2006GL028048.

Maineult, A., Strobach, E. & Renner, J., 2008. Self-potential signals induced by periodic pumping tests, J. Geophys. Res., 113, B01203, doi: 10.1029/2007JB005193.

Maineult, A., 2016. Estimation of the electrical potential distribution along metallic casing from surface self-potential profile, *J. Appl. Geophys.*, **129**, 66–78, doi: 10.1016/j.jappgeo.2016.03.038.

Nourbehecht, B., 1963. Irreversible thermodynamic effects in inhomogeneous media and their applications in certain geoelectric problems, *Ph.D. Thesis*, MIT, Cambridge, Ma.

Perrier, F. & Morat, P., 2000. Characterization of electrical daily variations induced by capillary flow in the non-saturated zone, *Pure Appl. Geophys.*, **157**, 785–810, doi: 10.1007/PL00001118.

Press, W.H., Flannery, B.P., Teukolsky, S.A. & Vetterling, W.T., 1992. *Numerical Recipes in C. The Art of Scientific Computing (2nd edition)*, Cambridge University Press, Cambridge, Ma.

Rasmussen, T.C., Haborak, K.G. & Young, M.H., 2003. Estimating aquifer hydraulic properties using sinusoidal pumping at the Savannah River site, South Carolina, USA, *Hydrogeol. J.*, **11**, 466–482, doi: 10.1007/s10040-003-0255-7.

Renner, J. & Messar, M., 2006. Periodic pumping tests, *Geophys. J. Int.*, **167**, 479–493, doi: 10.1111/j.1365-246X.2006.02984.x.

Revil, A. & Linde, N., 2006. Chemico electro-mechanical coupling in microporous media, *J. Coll. Interface Sci.*, **302**, 682–694, doi: 10.1016/j.jcis.2006.06.051.

Revil, A., Gévaudan, C., Lu, N. & Maineult, A., 2008. Hysteresis of the self-potential response associated with harmonic pumping tests, *Geophys. Res. Lett.*, **35**, L16402, doi:

10.1029/2008GL035025.

Rizzo, E., Suski, B., Revil, A., Straface, S. & Troisi, S. 2004. Self-potential signals associated with pumping tests experiments, *J. Geophys. Res.*, **109**, B10203, doi: 10.1029/2004JB003049.

Soueid Ahmed, A., Jardani, A., Revil, A. & Dupont, J.-P., 2016. Joint inversion of hydraulic head and self-potential data associated with harmonic pumping tests, *Water Resources Res.*, **52**, 6769–6791, doi: 10.1002/2016WR019058.

Tarasov, A. & Titov, K., 2007. Relaxation time distribution from time domain induced polarization measurements, *Geophys. J. Int.*, **170**, 31–43. doi: 10.1111/j.1365-246X.2007.03376.x.

Titov, K., Revil, A., Konosavsky, P., Straface, S. & Troisi, S., 2005. Numerical modelling of self potential signals associated with a pumping test experiment, *Geophys. J. Int.*, **162**, 641–650, doi: 10.1111/j.1365-246X.2005.02676.x.

Titov, K., Konosavsky, P. & Narbut, M., 2015. Pumping test in a layered aquifer: Numerical analysis of self-potential signals, *J. Appl. Geophys.*, **123**, 188–193, doi: 10.1016/j.jappgeo.2015.10.006.